BNUT

Iranian (Iranica) Journal of Energy & Environment
Journal Homepage: www.ijee.net
IJEE an official peer review journal of Babol Noshirvani University of Technology, ISSN:2079-2115

Thermodynamic Modeling and Analysis of a Solar and Geothermal-driven Multigeneration System Using TiO_2 and SiO_2 Nanoparticles

A. Habibzadeh[1], M. Abbasalizadeh*[1], I. Mirzaee[1], S. Jafarmadar[1], H. Shirvani[2]

[1] *Department of Mechanical Engineering, Engineering Faculty, Urmia University, Urmia, Iran*
[2] *Faculty of Science and Engineering, Anglia Ruskin University, Chelmsford, UK*

P A P E R I N F O

Paper history:
Received 22 October 2022
Accepted in revised form 09 December 2022

Keywords:
Geothermal
Kalina cycle
Multigeneration
Nanofluid
Solar collector

A B S T R A C T

In this study, renewable energy sources include a high-temperature solar parabolic trough collector and geothermal water integrated with a modified Kalina cycle, a combined ORC-ERC cycle, an electrolyzer, an RO desalination unit, and a domestic water heater were investigated. SiO_2 and TiO_2 nanoparticles dissolved in Therminol VP1 were applied as the working fluid of the solar collector. A comparative analysis of introduced working fluids is performed from energy, exergy as well as cost analysis point of view to evaluate their efficiencies. Solar irradiation, ambient temperature, and collector inlet temperature were the parameters investigated to discover their effects on energy and exergy efficiency, solar collector outlet temperature, hydrogen production rate, and freshwater production rate. The highest generated outlet temperature of the solar collector outlet was 693.8 K obtained by Therminol VP1/SiO_2 nanofluid. The maximum energy and exergy efficiencies of the proposed system were 36.69 % and 17.76 %, respectively. Moreover, it is found that by increasing the solar collector inlet temperature, the hydrogen production rate decreases while the water production rate increases.

***doi**: 10.5829/ijee.2023.14.02.05*

NOMENCLATURE

A	Area (m^2)	$\dot{Z}$	Capital cost rate (\$/h)
C_p	Specific heat capacity (J/kgK)	**Subscripts**	
CRF	Capital recovery factor	*0*	Ambient
D	Collector diameter (m)	*1,2,…*	State points
E	Energy input (kW)	*a*	Anode
$\dot{E}x$	Exergy rate (W)	*ap*	Aperture
ex	Exergy (J/kg)	*avg*	Average
F	Faraday constant (C/mol)	*c*	Cathode
F_1	Collector efficiency factor	*ch*	Chemical
F_R	Heat transfer factor	*con*	Condenser
G	Solar irradiation (W/m^2)	*cooling*	Cooling
h	Heat transfer coefficient (W/m^2K)	*D*	Destroyed
J	Current density (A/m^2)	*DWH*	Domestic water heater
J^a_{ref}	Pre-exponential factor (A/m^2)	*eje*	Ejector
J_O	Exchange current density (A/m^2)	*eva*	Evaporator
k	Thermal conductivity (W/m K)	*exv*	Expansion valve
K	The ratio of specific heats (C_P/C_V)	*HX*	Heat exchanger

*Corresponding Author Email: m.abbasalizadeh@urmia.ac.ir (M. Abbasalizadeh)

Please cite this article as: A. Habibzadeh, M. Abbasalizadeh, I. Mirzaee, S. Jafarmadar, H. Shirvani, 2023. Thermodynamic Modeling and Analysis of a Solar and Geothermal-driven Multigeneration System Using TiO_2 and SiO_2 Nanoparticles, Iranian (Iranica) Journal of Energy and Environment, 14(2), pp. 127-138. Doi: 10.5829/ijee.2023.14.02.05

L	Collector length (m)	mx	Mixer
M	Molecular weight (kg/mol)	net	Net
$\dot{m}$	Mass flow rate (kg/s)	ph	Physical
n_{cs}	Number of collectors in series	p	Pump
n_{cp}	Number of collectors in parallels	PEM	Proton exchange membrane
$\dot{N}$	Outlet flow rate of fluid x (kg/s)	PTC	Parabolic trough collector
P	Pressure (bar)	r	Receiver tube
$\dot{Q}$	Heat transfer rate (W)	re	Recuperator
Q_u	Useful energy gain	RO	Reverse osmosis
R	Overall ohmic resistance	sep	Separator
RR	Recovery ratio	sol	Solar
S	Absorbed solar radiation	spl	Splitter
T	Temperature (K)	t	Turbine
TCF	Temperature correction factor	th	Thermal
U_L	Solar collector's overall heat loss coefficient	vg	Vapor generator
V	Overpotential (V)	**Greek Symbols**	
V_O	Reversible potential (V)	$\sigma(x)$	Ionic conductivity of the membrane
V_{Ohm}	Ohmic overpotential of the electrolyte (V)	η	Efficiency
w	Collector width (m)	$\lambda(x)$	Water content at location x
$\dot{W}$	Net output power (kW)	ρ	Density (kg/m^3)
X	Salt concentration (g/kg)	ϕ	Concentration ratio
Z	Investment cost ($)		

INTRODUCTION

Two major concerns of society are increasing energy claims and applying fossil fuels [1]. Utilizing renewable energies which are clean and environmentally friendly is crucial to combat the adverse effects of hydrocarbon. Solar energy and geothermal energy are two types of renewable energies that can cope with the global warming problem [2]. Moreover, the design of novel high-efficiency systems such as multigeneration systems has attracted much attention [3]. Both of these sources are capable of integrating with other cycles to produce power. Utilizing this technology, due to the reduction of many losses that occur when converting thermal energy into mechanical or electrical, can not only significantly increase efficiency but also reduce environmental impact and overall system costs [4].

Al-Ali and Dincer [5] proposed a novel geothermal-solar system producing power, cooling, heating, heat, and hot water. The results showed a 60% and 10% difference between energy and exergy efficiencies when considering sole generation and the proposed multigeneration system. Waseem et al. [6] analyzed a solar-geothermal multigeneration system producing hydrogen, power, and cooling. The proposed cycle included an electrolyzer, Rankine cycle, and vapor absorption cycle. Two arrangements were comparatively investigated, and a 0.45% power efficiency difference was observed. Li et al. [7] developed a system including a geothermal cycle, solar cycle, and PEM system. The system generated electricity, hydrogen, heating, and hot water. To find the irreversibility, energy, and exergy analyses were done. Compared to the sole geothermal system, the proposed system can produce 148.3% more power.

To improve the performance of solar collectors, experts have introduced nanofluids that show high heat transfer properties. Nanofluids which are innovative heat transfer fluids are formed by dispersing nanoparticles smaller than 100 nm in standard working fluids [8]. One of the first comprehensive studies on the development of nanofluids was performed by Li et al. [9]. They carried out a numerical and experimental investigation as well as tried different preparation techniques to find out the effects of adding nanoparticles on the heat transfer properties of the base fluids. Toghyani et al. [10] studied a solar-based combined system using nanofluid as a working fluid for cooling and hydrogen production. The effects of different parameters on the performance of the system were examined. The results revealed that by using higher volume fractions of nanoparticles, the amount of the power and hydrogen produced by the system increases. Ratlamwala et al. [11] studied applying Al_2O_3- and Fe_2O_3-based nanofluids in the solar-geothermal multigeneration system. A comprehensive analysis of the used working fluids showed that Al_2O_3-based water nanofluid resulted in higher efficiency. Moreover, by increasing the nanoparticle percentage, the amount of hydrogen production rate and power generation decreased. Three different collector types-bare tube, non-evacuated receiver, and evacuated receiver- were studied by Bellos et al. [12] for investigating the thermal enhancement by using Syltherm 800/Cu nanofluid. According to the results, the bare tube showed the highest performance enhancement compared with other kinds. Ghasemi and Ranjbar [13] performed a comparative study between water-based nanofluids and it is discovered that the water/CuO leads to a 35% heat transfer coefficient increase, while this amount is 2% for water/Al_2O_3. Ibrahim and Kayfeci [14] studied the thermodynamic analysis of a trigeneration system driven by a parabolic trough solar collector based on two different types of nanofluid including graphene and ferrofluid added to Syltherm 800. The results proved that the system performance improves by applying nanofluids. Moreover, graphene nanoparticles show better results than ferrofluid nanoparticles. The authors stated that by using Syltherm 800/graphene nanofluid, the maximum collector outlet temperature is attained. Alashkar and Gadalla [15] investigated the application of nanofluid-based solar PTSC to run the Rankine cycle. They reported a slight increase in the annual energy output using Syltherm 800 and Therminol VP-1 as the base fluids and Cu, Al_2O_3, and SWCNT as the nanoparticles. The thermodynamic analysis of a PTC receiver tube using oil–Al_2O_3 nanofluid with a concentration ratio of 86 was investigated by Mwesigye et al. [16] applying the entropy generation minimization method. The authors proved that by varying the nanofluid temperature from 350 to 600 K, the thermal efficiency of the PTC increased by up to 7.6%. The volume fraction rising led to a reduction in the optimal Reynolds number. Khan et al. [17] studied the effect of applying nanofluids in a solar-based cycle from an energy, exergy, and exergo-environmental point of view. The influence of three nanofluids, including Fe_2O_3/Therminol VP1, SiO_2/Therminol VP1, and Cu/Therminol VP1, were compared by considering different parameters. The results showed that among the studied nanofluids, SiO_2/VP1 presented better outcomes. Moreover, the amount of CO_2 was reduced for all the studied nanofluids. Increasing nanoparticle concentration leads to an increment in the exergy efficiency and a decrease in the nanoparticle thermal conductivity. Ibrahim and Kayfeci [14] studied using two kinds of nanofluids in a parabolic trough solar collector of a trigeneration system. The results showed that by using ferrofluid and graphene as the nanoparticles, the overall performance of the proposed system improved. Graphene nanoparticles indicated better performance in comparison with ferrofluid nanoparticles. Kalbande et al. [18] studied the possibility of attaining a higher temperature range of above 200°C in oil-based thermal energy storage systems. They used aluminum oxide (Al_2O_3) and soybean oil nanofluid as the heat transfer fluid to store and transfer the sensible heat. After a mathematical analysis, they could achieve up to 220°C in a parabolic trough solar collector coupled with a thermal storage system. Tonekaboni et al. [19] studied the amount of enhancement of the solar collectors by adding porous media and nanofluid. They applied 90% porosity copper, CuO, and Al_2O_3 nanofluids to investigate the changing in the thermal properties of different types of solar collectors. The results showed that adding porous media and nano-fluids increased an average of 14.4% collector energy efficiency and 8.08% collector exergy efficiency. Moreover, the highest amount of energy and exergy efficiencies were 60.12% and 18.84%, respectively which were obtained for parabolic solar collectors. Said et al. [20] surveyed a nanofluid-based parabolic trough collector from energy, exergy, economic, and environmental points of view. The results showed that by adding Ti_3C_2 to the silicon oil, the thermal conductivity of the nanofluid enhances from 70 % to 89%. It is found that, compared to pure oil, applying nanofluid reduces the system's cost by 0.021M$ and increases the gained energy by 1.51%. For energy analysis, the annual CO_2 reduction varies from 2.25 to 2.30 tons CO_2/year.

Previous literature reviews have shown that there is an increasing interest in using different types of nanofluids in solar collectors to enhance their thermal efficiencies. Moreover, a few studies have been performed on the effects of SiO_2 and TiO_2 nanoparticles on multigeneration systems. On the other hand, publications about the efficiency study of nanofluids in high-temperature PTCs are rare. Moreover, to the best knowledge of the authors, there is no study of the combination of high-temperature Kalina cycle and nanofluid applied parabolic trough solar collectors. Therefore, this research aims to investigate an integrated system including solar and geothermal sources in which SiO_2 -based and TiO_2-based Therminol VP1 nanofluids have been applied as the PTC working fluids. This proposed design uses a high-temperature PTC, a geothermal water source, a modified Kalina cycle combined with an electrolyzer, a combined organic Rankine cycle and ejector refrigeration cycle, an RO desalination unit, and a domestic water heater.

A summary of the main goals and innovations of this study is presented below:

- Introducing a new multigeneration energy system using solar and geothermal renewable sources.
- Applying a modified high-temperature Kalina cycle for retrieving the solar source energy.
- Energy and exergy analysis of the proposed systems are applied to perform a comprehensive evaluation of the system.
- Comparing the use of three working fluids to analyze the performance of the system.
- Producing hydrogen and fresh water from the novel energy system.

SYSTEM DESCRIPTION

Figure 1 illustrates the schematic diagram of the proposed novel geothermal-solar multigeneration system. The presented system integrates solar parabolic collectors and a geothermal source with a modified Kalina cycle, a combined ORC-ERC cycle, an RO desalination unit, a PEM electrolyzer, and a domestic water heater. The solar collectors transform solar irradiation into useful heat by applying ThermінolVP1- SiO_2 and TherminolVP1- TiO_2 nanofluids as absorption medium and operates as the energy source of the Kalina cycle. In the Kalina cycle, two recuperators are employed to increase internal heat recovery and enhance the overall system efficiency. The thermal energy of the solar collector is transferred to the ammonia-water mixture in the evaporator. The superheated ammonia-water mixture expands through the turbine and goes to mixer 1 after passing the recuperators 1 and 2. In mixer 1 it gets mixed with the ammonia lean liquid from the separator to reduce the ammonia mass fraction in condenser 1. After passing the condenser and pump, a part of the basic solution goes to the splitter where it is separated into vapor and liquid streams. The remaining part of the basic solution is mixed with the ammonia-rich vapor coming from the separator in mixer 2 to form the working fluid again. This working fluid goes through the condenser 2 and pump to attain the high pressure required at the turbine inlet. The power produced in the turbine is applied to the electricity supply of a residential area and the source power of the RO desalination unit to generate freshwater. The temperature of the geothermal water rises by passing through the solar system heat exchanger. Then it enters the vapor generator of the combined ORC-ERC cycle and domestic water heater before discharging to the reinjection well. The ORC-ERC subsystem uses Isopentane as the working fluid. In the ORC-ERC cycle, the saturated liquid working fluid is pumped to the turbine after its temperature is increased by passing through the preheater and vaporized by absorbing heat from the geothermal heat source in the vapor generator. The partially expanded extracted vapor enters the ejector. The stream leaving the ejector is mixed with the fully expanded stream leaving the turbine and the resulting low-pressure vapor is cooled

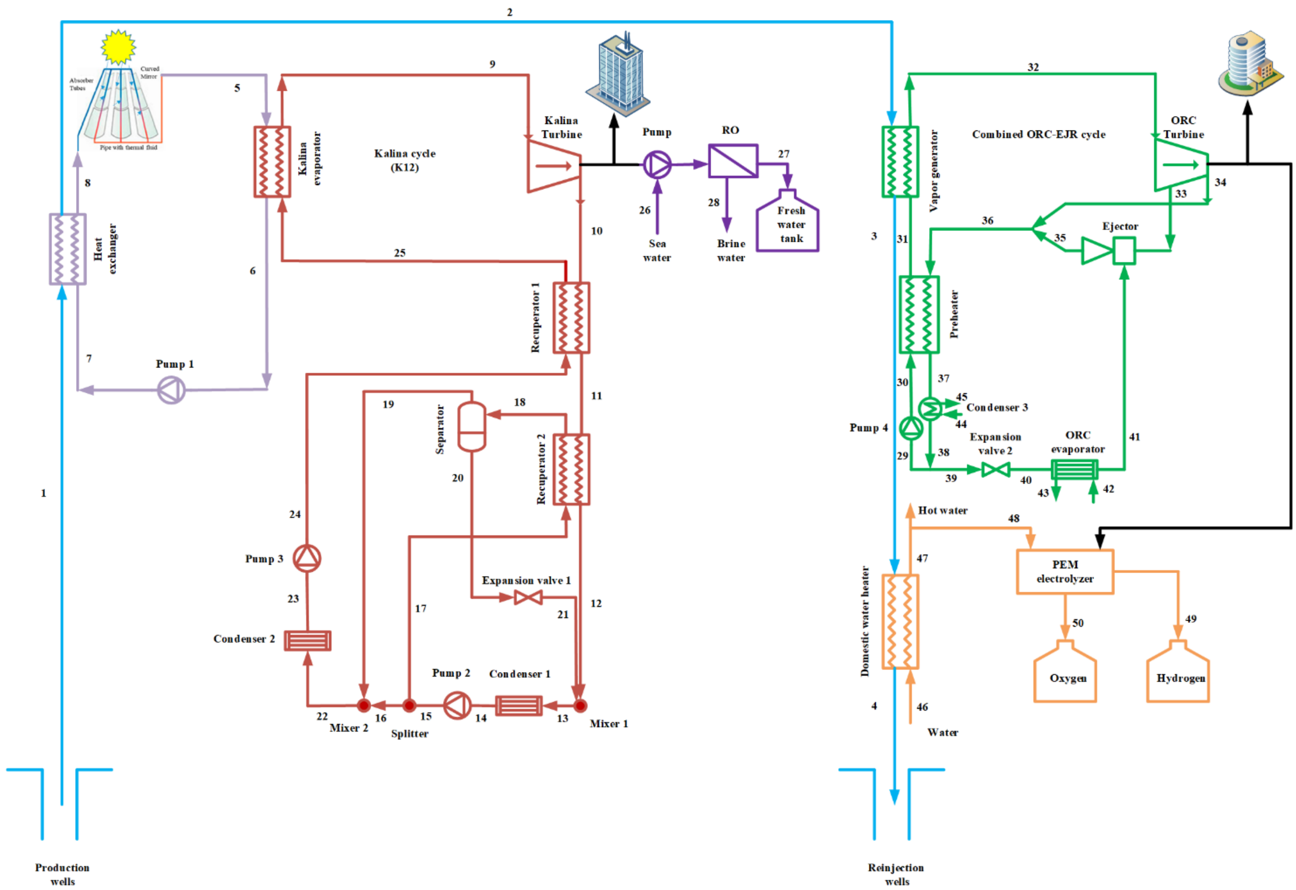

Figure 1. Schematic diagram of the proposed multigeneration system

in the preheater and liquefied by rejecting heat to the cooling water. The working fluid leaves the condenser as a saturated liquid and is divided into two streams. One stream returns to the pump and the other enters the evaporator after a pressure reduction in the expansion valve. The flow that enters the evaporator is vaporized by absorbing heat from the cooling medium to produce the required cooling effect and is then entrained into the ejector. The power generated by the ORC is employed in a residential area and delivered to a PEM electrolyzer to supply the required energy for hydrogen production. The results of the proposed system are electricity, fresh water, hydrogen, hot water, heating, and cooling.

THERMODYNAMIC MODELING

The current section presents the required mathematical equations for the simulation of the integrated system. EES software [21] has been applied to formulate and solve equations. The following considerations are considered to simplify the modeling process [22]:

- The system functions at a steady state.
- The pressure losses through the pipes and other components are ignored.
- The outlet streams of the condensers and evaporators are saturated liquid and saturated vapor, respectively.
- The rich vapor and the weak solution outlets from the separators are saturated vapor and saturated liquid, respectively.
- Solar radiation is considered to be uniform and geothermal water is presumed to be net water.

Table 1 indicates the nanoparticles' thermodynamic properties. In addition, Table 2 exhibits the primary input data used for coding, and Table 3 shows the equations required for modeling the different components of the proposed cycle.

Thermodynamic modeling is carried out by applying the conservation equations, the energy conservation, and the exergy balance equation [38].

$$\sum \dot{m}_i - \sum \dot{m}_e = 0 \tag{1}$$

$$\sum \dot{m}_i h_i - \sum \dot{m}_e h_e + \sum \dot{Q} - \sum \dot{W} = 0 \tag{2}$$

$$\sum \dot{Q}_k \left(1 - \frac{T_0}{T_k}\right) + \sum \dot{m}_i ex_i = \sum \dot{m}_e ex_e + \sum \dot{W} + \dot{E}x_{D,K} \tag{3}$$

Table 1. Thermophysical properties of the studied nanoparticles

Nanoparticle	$\rho (kg/m^3)$	$k (W/mK)$	$C_p (J/kgK)$
SiO_2 [23]	2220	1.4	745
TiO_2 [24]	4250	8.9	686

Table 2. Input data used in the simulation

Parameters	Unit	Value
Geothermal [25, 26]		
Production well temperature	$(^{\circ}C)$	120
Production well Pressure	(bar)	7
Solar [27-29]		
Collector width	(m)	5.76
Collector length	(m)	12.27
Receiver outside diameter	(m)	0.07
Receiver inside diameter	(m)	0.066
Collector heat loss coefficient	$(W/m^{2\circ}C)$	3.82
Receiver inlet temperature	$(^{\circ}C)$	180
The heat transfer coefficient inside the receiver	$(W/m^{2\circ}C)$	300
The thermal conductivity of the receiver	$(W/m^{2\circ}C)$	16
Solar radiation intensity	$(W/m^{2\circ}C)$	850
Cover glazing transmissivity	-	0.96
PTC effective transmissivity	-	0.94
Receiver absorptivity	-	0.96
Correction factor for diffuse radiation	-	0.95
volumetric nanoparticle concentration	$(\%)$	6
Kalina [30]		
Turbine inlet ammonia concentration	-	0.49
Turbine inlet temperature	$(^{\circ}C)$	330
Turbine inlet pressure	(bar)	120
RO [31, 32]		
Recovery ratio	-	0.3
Number of elements	-	7
Number of pressure vessels	-	42
Seawater salinity	(g/kg)	43
ORC-ERC [33-35]		
Turbine inlet pressure	(bar)	6.5
Evaporator temperature	$(^{\circ}C)$	-5

where, $\dot{E}x_{D,K}$, $\sum \dot{Q}_k \left(1-\frac{T_0}{T_k}\right)$ and $\sum \dot{W}$are the exergy destruction rate, heat transfer, and power exergy, respectively. The physical and chemical exergies are calculated as follows:

$$ex = ex_{ph} + ex_{ch} \quad (4)$$

$$ex_{ph} = \left[\left(h_i - h_o\right) - T_o\left(s_i - s_o\right)\right] \quad (5)$$

$$ex_{ch} = \left[\left(\frac{x}{M_{NH3}}\right)ex^o_{ch,NH3} + \left(\frac{1-x}{M_{H_2O}}\right)ex^o_{ch,H_2O}\right] \quad (6)$$

where, x is the molar fraction of ammonia [39].

Moreover, the amount of investment for each component of the cycle can be defined as follows [40].

$$\dot{Z}_K = \frac{Z_K \times \varphi \times CRF}{N} \quad (7)$$

where,φ is the operation and maintenance factor which is assumed as 1.06. The annual time operation of the system is shown with N, which is assumed as 8000.

In addition, CRF is the capital recovery factor and is expressed by [31].

$$CRF = \frac{i_r\left(1+i_r\right)^n}{\left(1+i_r\right)^n - 1} \quad (8)$$

here, i presents the interest rate and is 0.15 and n presents the expected life of the cycle elements and is n=20 years. By applying fundamental equations to all system components, the energy, exergy equations, and cost functions for all components of the proposed multigeneration system can be defined as listed in Tables 4 and 5.

RESULTS AND DISCUSSION

After defining all required equations and constants for simulating the high-temperature nanofluid-based PTC combined with a geothermal source system, in the following section, the outputs and results of the studied system assessment are presented through different tables and diagrams under varying different parameters. EES software was utilized to accomplish all thermodynamic computations. As the proposed multigeneration system is novel, therefore, to certify the accuracy of the modeling, some of the main parts of the system have been validated by previous studies. The verification of the PTC cycle was performed with the corresponding test results from SNL [41]. Table 6 summarizes a good coincidence between the present modeling and the previous findings.

Table 3. Equations required for modeling the components

Parabolic trough collector [29, 36]	
Useful energy obtained by the fluid	$Q_u = n_{cp} n_{cs} F_R A_{ap}[S - \frac{A_r}{A_{ap}} U_L (T_{r,i} - T_0)]$ $F_R = \frac{\dot{m}c_{p,c}}{A_r U_L}[1 - \exp(-\frac{A_r U_L F_1}{\dot{m}c_{p,c}})]$ $F_1 = \frac{\frac{1}{U_L}}{\frac{1}{U_L} + \frac{D_{o,r}}{h_{fi}} + (\frac{D_{0,r}}{2k}\ln\frac{D_{o,r}}{D_{i,r}})}$
The surface area of PTC	$A_a = (w - D)L$
RO unit [31]	
The recovery ratio	$RR = \frac{\dot{m}_{27}}{\dot{m}_{26}}$
Saline water flow rate	$\dot{m}_{28} = \dot{m}_{26} - \dot{m}_{27}$
Osmotic pressure	$P_{net} = P_{avg,f} - 75.85 \times X_{27}$
Average Osmosis pressure	$P_{avg,f} = \frac{P_{26} + P_{28}}{2} = 37.92 \times \left(X_{26} + X_{28}\right)$
Temperature correction factor	$TCF = \exp\left\{2700 \times \left(\frac{1}{T+273} - \frac{1}{298}\right)\right\}$
Membrane water permeability	$K_w = \frac{6.84 \times 10^{-8} \times \left(18.6865 - 0.177 \times X_{28}\right)}{\left(T + 273\right)}$
High-pressure pump power	$\dot{W}_{p,RO} = \frac{\dot{m}_{26} \times \Delta P}{\rho_{26} \times \eta_p}$
PEM [37]	
Electrical energy consumption	$\dot{E}_{electric} = JV$
Electrolyzer voltage	$V = V_0 + V_{act,c} + V_{act,a} + V_{ohm}$
Reversible equation	$V_0 = 1.229 - 0.00085(T_{PEM} - 298)$
Activation overpotential	$A_{act,i} = \frac{RT}{F}\sinh^{-1}\left(\frac{J}{2J_{0,i}}\right) =$ $J_a^{ref}\exp\left(\frac{-E_{act,i}}{RT}\right), i = a, c$
Ohmic overpotential	$V_{ohm} = JR_{PEM}, R_{PEM} =$ $\int_0^L \frac{dx}{\sigma\left[\lambda\left(x\right)\right]}, \lambda\left(x\right) = \frac{\lambda_a - \lambda_c}{D}x + \lambda_c$ $\sigma\left[\lambda\left(x\right)\right] = \left[0.5139\lambda\left(x\right) - 0.326\right]$ $\exp\left[1268\left(\frac{1}{303} - \frac{1}{T}\right)\right]$
Rate of produced H_2	$\dot{N}_{H_2,Out} = \frac{J}{2F} = \dot{N}_{H_2O,reacted}$

Table 4. Energy and exergy equations for the system components

Components	Energy equations	Exergy equations
PTC field	$\dot{m}_8 h_8 + \dot{Q}_u = \dot{m}_5 h_5$	$\dot{E}x_{D,PTC} = \dot{E}x_{sun} + \dot{E}x_8 - \dot{E}x_5$
Heat exchanger	$\dot{Q}_{HX} = \dot{m}_1(h_2 - h_1) = \dot{m}_7(h_7 - h_8)$	$\dot{E}x_{D,HX} = \dot{E}x_1 + \dot{E}x_7 - \dot{E}x_2 - \dot{E}x_8$
Kalina evaporator	$\dot{Q}_{eva,KAL} = \dot{m}_5(h_5 - h_6) = \dot{m}_9(h_9 - h_{25})$	$\dot{E}x_{D,eva,KAL} = \dot{E}x_5 + \dot{E}x_{25} - \dot{E}x_6 - \dot{E}x_9$
Kalina turbine	$\dot{W}_{t,KAL} = \dot{m}_9(h_9 - h_{10})$	$\dot{E}x_{D,t,KAL} = \dot{E}x_9 - \dot{W}_{t,KAL} - \dot{E}x_{10}$
Kalina recuperator 1	$\dot{Q}_{re1,KAL} = \dot{m}_{10}(h_{10} - h_{11}) = \dot{m}_{24}(h_{25} - h_{24})$	$\dot{E}x_{D,re1,KAL} = \dot{E}x_{10} + \dot{E}x_{24} - \dot{E}x_{11} - \dot{E}x_{25}$
Kalina recuperator 2	$\dot{Q}_{re2,KAL} = \dot{m}_{11}(h_{11} - h_{12}) = \dot{m}_{17}(h_{18} - h_{17})$	$\dot{E}x_{D,re2,KAL} = \dot{E}x_{11} + \dot{E}x_{17} - \dot{E}x_{12} - \dot{E}x_{18}$
Kalina mixer 1	$\dot{m}_{12}h_{12} + \dot{m}_{21}h_{21} = \dot{m}_{13}h_{13}$	$\dot{E}x_{D,mx1,KAL} = \dot{E}x_{12} + \dot{E}x_{21} - \dot{E}x_{13}$
Kalina mixer 2	$\dot{m}_{16}h_{16} + \dot{m}_{19}h_{19} = \dot{m}_{22}h_{22}$	$\dot{E}x_{D,mx2,KAL} = \dot{E}x_{16} + \dot{E}x_{19} - \dot{E}x_{22}$
Kalina condenser 1	$\dot{Q}_{con1,KAL} = \dot{m}_{13}(h_{13} - h_{14})$	$\dot{E}x_{D,con1,KAL} = \dot{E}x_{13} - \dot{E}x_{14} - \dot{Q}_{con1,KAL}\left(1 - \frac{T_0}{T_{14}}\right)$
Kalina condenser 2	$\dot{Q}_{con2,KAL} = \dot{m}_{22}(h_{22} - h_{23})$	$\dot{E}x_{D,con2,KAL} = \dot{E}x_{22} - \dot{E}x_{23} - \dot{Q}_{con2,KAL}\left(1 - \frac{T_0}{T_{23}}\right)$
Kalina pump 2	$\dot{W}_{p2,KAL} = \dot{m}_{14}(h_{15} - h_{14})$	$\dot{E}x_{D,p2,KAL} = \dot{W}_{p2,KAL} + \dot{E}x_{14} - \dot{E}x_{15}$
Kalina pump 3	$\dot{W}_{p3,KAL} = \dot{m}_{23}(h_{24} - h_{23})$	$\dot{E}x_{D,p3,KAL} = \dot{W}_{p3,KAL} + \dot{E}x_{23} - \dot{E}x_{24}$
Kalina splitter	$\dot{m}_{15}h_{15} = \dot{m}_{16}h_{16} + \dot{m}_{17}h_{17}$	$\dot{E}x_{D,spl,KAL} = \dot{E}x_{15} - \dot{E}x_{16} - \dot{E}x_{17}$
Kalina separator	$\dot{m}_{18}h_{18} = \dot{m}_{19}h_{19} + \dot{m}_{20}h_{20}$	$\dot{E}x_{D,sep,KAL} = \dot{E}x_{18} - \dot{E}x_{19} - \dot{E}x_{20}$
Kalina expansion valve 1	$h_{20} = h_{21}$	$\dot{E}x_{D,exv1,KAL} = \dot{E}x_{20} - \dot{E}x_{21}$
ORC vapor generator	$\dot{Q}_{vg,ORC-ERC} = \dot{m}_2(h_2 - h_3) = \dot{m}_{31}(h_{32} - h_{31})$	$\dot{E}x_{D,vg,ORC-ERC} = \dot{E}x_2 + \dot{E}x_{31} - \dot{E}x_3 - \dot{E}x_{32}$
ORC turbine	$\dot{W}_{t,ORC-ERC} = \dot{m}_{32}(h_{32} - h_{33}) + \dot{m}_{34}(h_{33} - h_{34})$	$\dot{E}x_{D,t,ORC-ERC} = \dot{E}x_{32} - \dot{W}_{t,ORC-ERC} - \dot{E}x_{33} - \dot{E}x_{34}$
ORC ejector	$\mu_{eje} = \frac{\dot{m}_{41}}{\dot{m}_{33}}$	$\dot{E}x_{D,eje,ORC-ERC} = \dot{E}x_{33} + \dot{E}x_{41} - \dot{E}x_{35}$
ORC preheater	$\dot{Q}_{ph,ORC-ERC} = \dot{m}_{30}(h_{31} - h_{30}) = \dot{m}_{36}(h_{36} - h_{37})$	$\dot{E}x_{D,ph,ORC-ERC} = \dot{E}x_{30} + \dot{E}x_{36} - \dot{E}x_{31} - \dot{E}x_{37}$
ORC pump 4	$\dot{W}_{p,ORC-ERC} = \dot{m}_{29}(h_{30} - h_{29})$	$\dot{E}x_{D,p4,ORC-ERC} = \dot{W}_{p4,ORC-ERC} - \dot{E}x_{29} + \dot{E}x_{30}$
ORC condenser 3	$\dot{Q}_{con3,ORC-ERC} = \dot{m}_{37}(h_{37} - h_{38}) = \dot{m}_{44}(h_{45} - h_{44})$	$\dot{E}x_{D,con3,ORC-ERC} = \dot{E}x_{37} + \dot{E}x_{44} - \dot{E}x_{38} - \dot{E}x_{45}$
ORC expansion valve 2	$h_{39} = h_{40}$	$\dot{E}x_{D,exv2,ORC-ERC} = \dot{E}x_{39} - \dot{E}x_{40}$
ORC evaporator	$\dot{Q}_{eva,ORC-ERC} = \dot{m}_{40}(h_{41} - h_{40})$	$\dot{E}x_{D,eva,ORC-ERC} = \dot{E}x_{40} + \dot{E}x_{42} - \dot{E}x_{41} - \dot{E}x_{43}$
PEM	$\dot{W}_{PEM} = (\dot{m}_{48}h_{48} - \dot{m}_{49}h_{49} - \dot{m}_{50}h_{50})$	$\dot{E}x_{D,PEM} = \dot{E}x_{48} + \dot{W}_{PEM} - \dot{E}x_{49} - \dot{E}x_{50}$
DWH	$\dot{Q}_{DWH} = \dot{m}_3(h_3 - h_4) = \dot{m}_{46}(h_{47} - h_{46})$	$\dot{E}x_{DWH} = \dot{E}x_3 + \dot{E}x_{46} - \dot{E}x_4 - \dot{E}x_{47}$
RO	$\dot{W}_{RO} = (\dot{m}_{26}h_{26} - \dot{m}_{27}h_{27} - \dot{m}_{28}h_{28})$	$\dot{E}x_{D,RO} = \dot{E}x_{26} - \dot{E}x_{27} - \dot{E}x_{28}$
Overall energy	$\eta_{th,tot} = \frac{\dot{W}_{KAL} + \dot{W}_{ORC-ERC} + \dot{Q}_{cooling} + \dot{Q}_{DWH} + \dot{m}_{49}HHV_{H2} - \dot{W}_{PEM} + \dot{m}_{27}h_{27} - \dot{W}_{RO}}{\dot{Q}_u + \dot{m}_1 h_1}$	
Overall exergy	$\eta_{ex,tot} = \frac{\dot{W}_{KAL} + \dot{W}_{ORC-ERC} + \dot{E}x_{cooling} + \dot{E}x_{43} + \dot{E}x_{50} + \dot{E}x_{47} - \dot{E}x_{46} + \dot{E}x_{27}}{\dot{E}x_{in,sun} + \dot{E}x_1}$	

Table 7 indicates the calculated parameters describing the solar system performance comparing the base fluid and two types of nanofluids. It becomes clear that adding nanoparticles to the base working fluid improves the solar system positively. Moreover, the mass flow rate rises in the PTSC receiver using nanoparticles. Among the proposed working fluids, by applying Therminol VP1/SiO_2, the maximum solar collector outlet temperature is achieved which is 656.6 K. Adding TiO_2 nanoparticle to the base fluid increases the collector efficiency. As it is displayed in the table, Therminol VP1/TiO_2 produces the highest net power, and thermal and exergy efficiencies.

Figure 2 shows the effect of solar irradiation on the overall energy and exergy efficiency of the multigeneration system. The graphs indicate that there is a negligible difference between the nanofluids for energy efficiency variation. Energy and exergy efficiencies of the system decrease with increasing solar irradiation. By increasing solar irradiation from 400 to 1000 W/m^2, the energetic efficiency of the multigeneration system decreases from 36.69% to 33.06%, while the exergetic efficiency reduces from 17.76% to 16.28%. It is clear that applying Therminol VP1/TiO_2 results in higher energy and exergy efficiencies. The reason for this increase is the high density and thermal capacity and low specific heat of TiO_2 nanofluid which results in higher energy absorption. Increasing solar irradiation leads to higher solar intensity bouncing back on the receiver, which increases the temperature of the nanofluids leaving the parabolic trough collector. The higher the nanofluid temperature leaving the receiver, the higher the efficiency of the PTC and more power will be produced in the turbines of Kalina and ORC cycles. When the solar irradiation rises, the ratio of the useful energy achieved from the collector is higher than the power produced by the system which decreases the efficiencies of the system.

The intensity of solar radiation has a considerable impact on the outlet temperature leaving the PTC. The effect of solar irradiance on the outlet temperature of the collector is shown in Figure 3. The evaluation of the figure makes it clear that for the studied nanofluids, the outlet temperature rises when the solar radiation intensity increases. Moreover, it is obvious that by adding nanoparticles to the base fluid, a higher outlet temperature is obtained. By changing the solar irradiation, the maximum outlet temperature can be achieved by using Therminol VP1/SiO_2 fluid which is 693.8 K. The higher the exit temperature of the solar collector, the higher the heat rate generated by the Kalina cycle evaporator.

Ambient temperature is one of the factors that affect the operation of the solar system. The effect of the ambient temperature on the outlet temperature of the solar collector is indicated in Figure 4. It is observed that the outlet temperature rises when the environmental temperature rises. The figure shows that ambient temperature has very little effect on the outlet temperature of the solar collector. By changing the ambient temperature from 283.15 to 333.15 K, the outlet temperature increases just 2.2 K. The highest outlet temperature is achieved by applying SiO_2-based nanofluid.

Figure 5 displays the effect of the solar collector inlet temperature on the overall energy and exergy efficiency

Table 5. The cost functions for the system components

Components	The cost functions [42, 43]
PTC field	$Z_{PTC} = 240 \times A_a$
Heat exchanger	$Z_{HX} = 130 \times (\frac{A_{HX}}{0.093})^{0.78}$
Kalina evaporator	$Z_{eva,KAL} = 1397 \times (A_{eva,KAL})^{0.89}$
Kalina turbine	$Z_{t,KAL} = 4450 \times (\dot{W}_{t,KAL})^{0.7}$
Kalina recuperator 1	$Z_{re1,KAL} = 130 \times (\frac{A_{re1,KAL}}{0.093})^{0.78}$
Kalina recuperator 2	$Z_{re2,KAL} = 130 \times (\frac{A_{re2,KAL}}{0.093})^{0.78}$
Kalina mixer 1	$Z_{mx1,KAL} = 0$
Kalina mixer 2	$Z_{mx2,KAL} = 0$
Kalina condenser 1	$Z_{con1,KAL} = 130 \times (\frac{A_{con1,KAL}}{0.093})^{0.78}$
Kalina condenser 2	$Z_{con2,KAL} = 130 \times (\frac{A_{con2,KAL}}{0.093})^{0.78}$
Kalina pump 2	$Z_{p2,KAL} = 1120 \times (\dot{W}_{p2,KAL})^{0.8}$
Kalina pump 3	$Z_{p3,KAL} = 1120 \times (\dot{W}_{p3,KAL})^{0.8}$
Kalina splitter	$Z_{spl,KAL} = 0$
Kalina separator	$Z_{sep,KAL} = 0$
Kalina expansion valve 1	$Z_{exv1,KAL} = 114.5 \times \dot{m}_{20}$
ORC vapor generator	$Z_{vg,ORC-ERC} = 1397 \times (A_{vg,ORC-ERC})^{0.89}$
ORC turbine	$Z_{t,ORC-ERC} = 4450 \times (\dot{W}_{t,ORC-ERC})^{0.7}$
(continued)	
ORC ejector	$Z_{eje,ORC-ERC} = 750 \times \dot{m}_{33} \times \left(\frac{T_{41}}{P_{41}}\right)^{0.05} \times (P_{36})^{-0.75}$
ORC preheater	$Z_{ph,ORC-ERC} = 130 \times (\frac{A_{ph,ORC-ERC}}{0.093})^{0.78}$
ORC pump 4	$Z_{p4,ORC-ERC} = 1120 \times (\dot{W}_{p4,ORC-ERC})^{0.8}$
ORC condenser 3	$Z_{con3,ORC-ERC} = 130 \times (\frac{A_{con3,ORC-ERC}}{0.093})^{0.78}$
ORC expansion valve 2	$Z_{exv2,ORC-ERC} = 114.5 \times \dot{m}_{39}$
ORC evaporator	$Z_{eva,ORC-ERC} = 130 \times (\frac{A_{ev,ORC-ERC}}{0.093})^{0.78}$
PEM	$Z_{PEM} = 1000 \times \dot{W}_{pem}$
DWH	$Z_{DWH} = 130 \times (\frac{A_{DWH}}{0.093})^{0.78}$
RO	$Z_{RO} = c_k \times n_v \times n_e + c_{pv} \times n_v + 996 \times (\dot{m}_{27})^{0.8}$

Table 6. Comparison of the results of the present work with the experimental results from SNL tests for the PTC field

T_{in} (°C)	T_{out} (°C)		Thermal Efficiency of PTC (%)	
	Present study	SNL test [41]	Present study	SNL test [41]
102.2	124.15	124	72.11	72.51
151	173.35	173.3	70.94	70.9
197.5	219.35	219.5	70.35	70.17
250.7	268.75	269.4	69.76	70.25
297.8	315.75	316.9	68.34	67.98

Table 7. System performance results for the proposed solar system working with different working fluids

Parameter	Therminol VP1	Therminol VP1/SiO_2	Therminol VP1/TiO_2
T_{out} $[K]$	655.5	656.6	649.8
η_c [%]	67.62	67.55	67.98
$\dot{Q}_u$ $[kW]$	6260	6254	6293
$\dot{E}x_{sol}$ $[kW]$	36725	36690	36901
ρ $[kgm^{-3}]$	930.8	1008	1130
C_p $[Jkg^{-1}K^{-1}]$	1.994	1.829	1.699
K $[Wm^{-1}K^{-1}]$	0.1049	0.1265	0.1312
$\dot{m}$ $[kgs^{-1}]$	15.51	16.80	18.83
W_{net} $[kW]$	1349	1348	1354
$\dot{Q}_{cooling}$ $[kW]$	526.5	526.5	526.5
η_{th} [%]	33.70	33.70	33.72
η_{ex} [%]	16.47	16.46	16.53
$\dot{m}_{H2}$ $[g/s]$	0.00164	0.00116	0.00118
$\dot{m}_{water}$ $[kg/s]$	4.848	4.848	4.849
$\dot{Z}$ [$/y]	140921	140814	141482

of the proposed multigeneration system. The results of the three different cases were investigated, including base fluid (Therminol VP1), TiO_2-based nanofluid, and SiO_2-based nanofluid. As can be inferred from the diagrams, for both energy and exergy efficiencies, Therminol VP1-TiO_2 nanofluid show higher values compared with other studied fluids. For energetic efficiency, as the inlet temperature increases from 443 K to 493 K, the amount of the net power produced by the system increases while the useful energy generated by the solar collector decreases. At first, the amount of energy produced is superior to the produced power and causes a decrease in the thermodynamic efficiency of the system, but then this superiority disappears and causes an increase in the efficiency. For TiO_2-based nanofluid, the thermal efficiency first decreases from 34.08 % to 33.51 % and then increases to 34.36 %. It can be seen that 468 K is an optimum point for the energetic efficiency graph. By analyzing the exergetic efficiency graph, it can be concluded that increasing the PTC inlet temperature, increases the exergy efficiency for all working fluids.

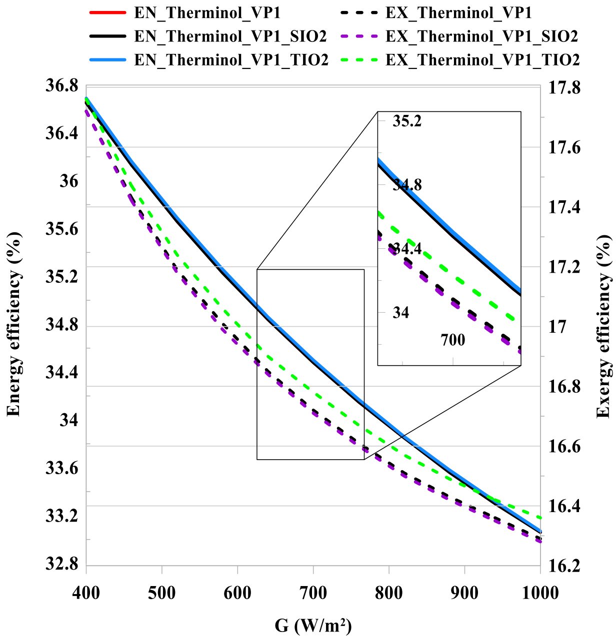

Figure 2. Effect of solar irradiation on energy and exergy efficiency

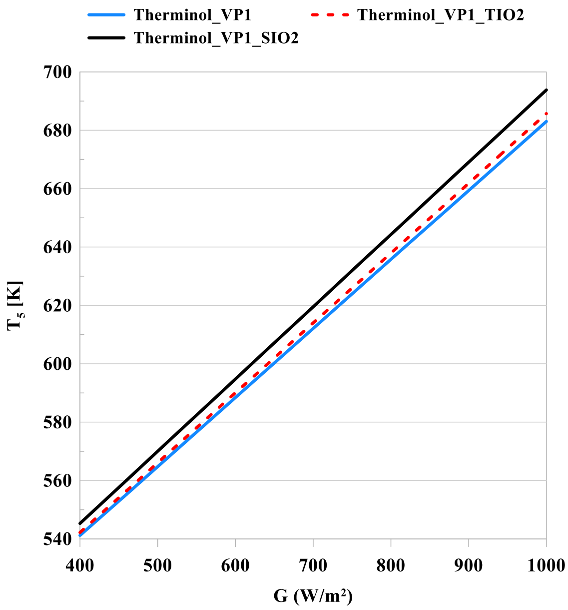

Figure 3. Effect of solar irradiation on the outlet temperature of the collector

Figure 6 displays the effect of the inlet temperature of the solar collector on the system's hydrogen production

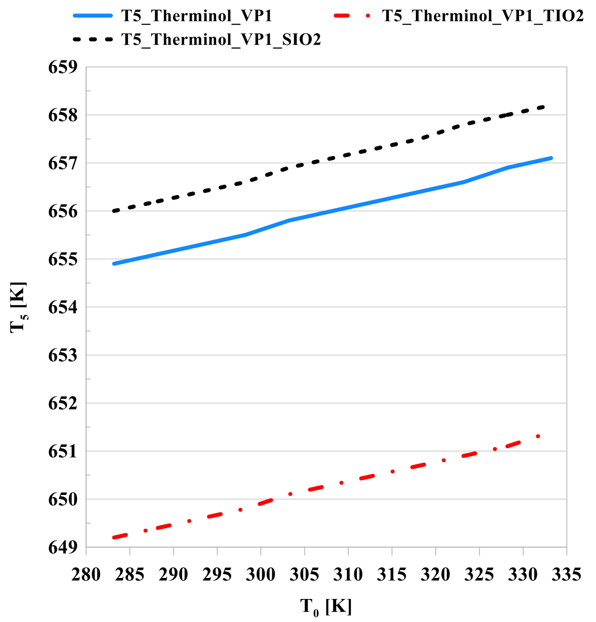

Figure 4. Effect of the ambient temperature on the outlet temperature of the collector

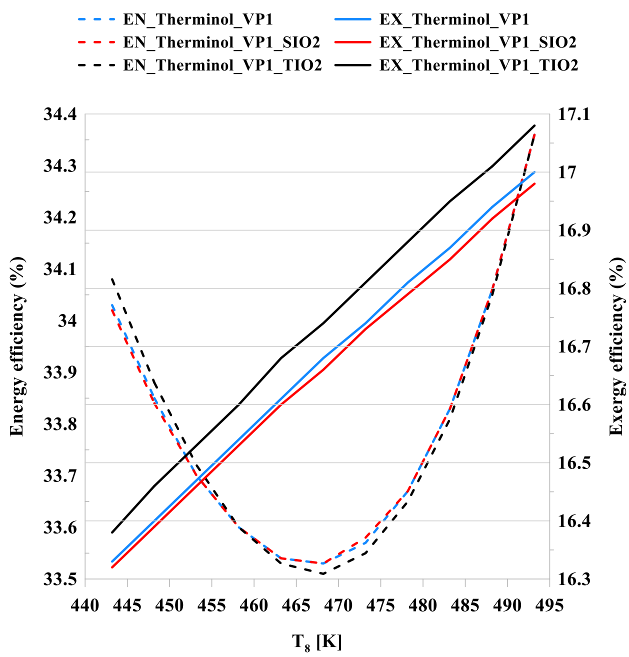

Figure 5. Effect of the collector inlet temperature on the energy and exergy efficiency

rate and freshwater production rate. According to the graphs, when the inlet temperature of the collector increases, the hydrogen production rate decreases while By analyzing the freshwater production rate increases. when the inlet temperature the results, it can be found that

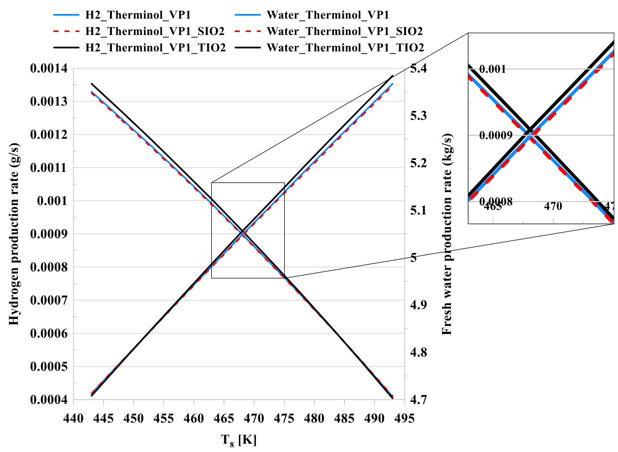

Figure 6. Effect of the collector inlet temperature on the hydrogen production and freshwater production rates

rises by about 11.2 %, the freshwater production rate increases by about 14.3 %, and the hydrogen production rate decreases by about 70 %. By comparing the graphs, Therminol VP1/TiO_2 nanofluid showed better results compared with other studied fluids.

CONCLUSION

In this research, a thermodynamic analysis was carried out to investigate the effect and possibility of using two types of nanofluids- TherminolVP1/ SiO_2 and TherminolVP1/TiO_2- in a multigeneration system comprising PTC and water geothermal sources. The system produces power, fresh water, hydrogen, hot water, heating, and cooling. The efficiency parameters of the thermodynamic analysis of the integrated system were computed. Some parameters were analyzed separately to find their effects on the system performance. A comparative investigation among the base fluid and two introduced nanofluids was done to find the most suitable working fluid for the solar collector. The summary of the important results is as follows:

- For all studied parameters except collector outlet temperature, TherminolVP1/ TiO_2 showed better performance compared with other fluids and resulted in higher values.
- Compared to the Therminol VP1 as the base fluids, applying TiO_2-nanoparticles leads to higher power production and better efficiency.
- When the solar irradiation varies from 400 to 1000 (W/m^2), overall energy and exergy efficiencies tend to decrease while the outlet temperature of the solar collector tends to increase.
- The maximum solar collector outlet temperature, 693.8 K is obtained by using TherminolVP1/ SiO_2 nanofluid.

- The highest amounts for energetic and exergetic efficiencies are achieved by using ThermінolVP1/ TiO_2 nanofluid which is 36.69% and 17.76 %, respectively.
- One of the parameters that affect the performance of the proposed system is ambient temperature. By changing the temperature from 283 to 333 K, the solar collector outlet temperature for all the studied working fluids increases.
- By varying the collector inlet temperature from 443 to 493 K, the hydrogen production rate decreases but exergy efficiency and freshwater production rate, increase. Moreover, for energy efficiency, an optimum point can be seen around 468 K.
- By adding TiO_2-nanoparticles, the solar collector efficiency and useful energy achieved by the collector increase.

REFERENCES

1. Martins, F., Felgueiras, C. and Smitková, M., 2018. Fossil fuel energy consumption in European countries, *Energy Procedia,* 153, pp. 107-111. Doi:10.1016/j.egypro.2018.10.050
2. Khorram, B., Mirzaee, I. and Jafarmadar, S., 2022. Thermoeconomic Analysis of Solar Chimney and Wind Turbine Application to Help Generate Electricity in a Trigeneration Cycle, *Iranian (Iranica) Journal of Energy & Environment,* 13(3), pp. 220-230. Doi:10.5829/ijee.2022.13.03.02
3. Aghagolzade, R., Jahanian, O. and Alizadeh Kharkeshi, B., 2022. Investigating a Combined cooling, heating and power system from energy and exergy point of view with RK-215 ICE engine as a prime mover, *Iranian (Iranica) Journal of Energy & Environment*. Doi:10.5829/IJEE.2023.14.01.09
4. Taheri, M., Mosaffa, A. and Farshi, L. G., 2017. Energy, exergy and economic assessments of a novel integrated biomass based multigeneration energy system with hydrogen production and LNG regasification cycle, *Energy,* 125, pp. 162-177. Doi:10.1016/j.energy.2017.02.124
5. Al-Ali, M. and Dincer, I., 2014. Energetic and exergetic studies of a multigenerational solar–geothermal system, *Applied Thermal Engineering,* 71(1), pp. 16-23. Doi:10.1016/j.applthermaleng.2014.06.033
6. Waseem, S., Ratlamwala, T. A. H., Salman, Y. and Bham, A. A., 2020. Geothermal and solar based mutligenerational system: a comparative analysis, *International Journal of Hydrogen Energy,* 45(9), pp. 5636-5652. Doi:10.1016/j.ijhydene.2019.06.135
7. Li, T., Qin, H., Wang, J., Gao, X., Meng, N., Jia, Y. and Liu, Q., 2021. Energetic and exergetic performance of a novel polygeneration energy system driven by geothermal energy and solar energy for power, hydrogen and domestic hot water, *Renewable Energy,* 175, pp. 318-336. Doi:10.1016/j.renene.2021.04.062
8. Olia, H., Torabi, M., Bahiraei, M., Ahmadi, M. H., Goodarzi, M. and Safaei, M. R., 2019. Application of nanofluids in thermal performance enhancement of parabolic trough solar collector: state-of-the-art, *Applied Sciences,* 9(3), pp. 463. Doi:10.3390/app9030463
9. Li, Y., Tung, S., Schneider, E. and Xi, S., 2009. A review on development of nanofluid preparation and characterization, *Powder Technology,* 196(2), pp. 89-101. Doi:10.1016/j.powtec.2009.07.025
10. Toghyani, S., Afshari, E., Baniasadi, E. and Shadloo, M., 2019. Energy and exergy analyses of a nanofluid based solar cooling and hydrogen production combined system, *Renewable Energy,* 141, pp. 1013-1025. Doi:10.1016/j.renene.2019.04.073
11. Ratlamwala, T. A. H., Waseem, S., Salman, Y. and Bham, A. A., 2019. Geothermal and solar energy–based multigeneration system for a district, *International Journal of Energy Research,* 43(10), pp. 5230-5251. Doi:10.1002/er.4480
12. Bellos, E., Tzivanidis, C. and Said, Z., 2020. A systematic parametric thermal analysis of nanofluid-based parabolic trough solar collectors, *Sustainable Energy Technologies and Assessments,* 39, pp. 100714. Doi:10.1016/j.seta.2020.100714
13. Ghasemi, S. E. and Ranjbar, A. A., 2016. Thermal performance analysis of solar parabolic trough collector using nanofluid as working fluid: a CFD modelling study, *Journal of Molecular Liquids,* 222, pp. 159-166. Doi:10.1016/j.molliq.2016.06.091
14. Ibrahim, A. and Kayfeci, M., 2021. Comparative analysis of a solar trigeneration system based on parabolic trough collectors using graphene and ferrofluid nanoparticles, *Thermal Science,* 25(4 Part A), pp. 2549-2563. Doi:10.2298/TSCI191103164I
15. Alashkar, A. and Gadalla, M., 2017. Thermo-economic analysis of an integrated solar power generation system using nanofluids, *Applied Energy,* 191, pp. 469-491. Doi:10.1016/j.apenergy.2017.01.084
16. Mwesigye, A., Huan, Z. and Meyer, J. P., 2015. Thermodynamic optimisation of the performance of a parabolic trough receiver using synthetic oil–Al2O3 nanofluid, *Applied Energy,* 156, pp. 398-412. Doi:10.1016/j.apenergy.2015.07.035
17. Khan, M. S., Amber, K. P., Ali, H. M., Abid, M., Ratlamwala, T. A. and Javed, S., 2020. Performance analysis of solar assisted multigenerational system using therminol VP1 based nanofluids: a comparative study, *Thermal Science,* 24(2 Part A), pp. 865-878. Doi:10.2298/TSCI180608062K
18. Kalbande, V. P., Walke, P. V. and Rambhad, K., 2021. Performance of oil-based thermal storage system with parabolic trough solar collector using Al2O3 and soybean oil nanofluid, *International Journal of Energy Research,* 45(10), pp. 15338-15359. Doi:10.1002/er.6808
19. Tonekaboni, N., Salarian, H., Nimvari, M. E. and Khaleghinia, J., 2021. Energy and exergy analysis of an enhanced solar CCHP system with a collector embedded by porous media and nano fluid, *Journal of Thermal Engineering,* 7(6), pp. 1489-1505. Doi:10.18186/thermal.990897
20. Said, Z., Ghodbane, M., Boumeddane, B., Tiwari, A. K., Sundar, L. S., Li, C., Aslfattahi, N. and Bellos, E., 2022. Energy, exergy, economic and environmental (4E) analysis of a parabolic trough solar collector using MXene based silicone oil nanofluids, *Solar Energy Materials and Solar Cells,* 239, pp. 111633. Doi:10.1016/j.solmat.2022.111633
21. Klein, S. A. and Alvarado, F., 2002. Engineering equation solver, *F-Chart Software, Madison, WI,* 1.
22. Musharavati, F., Khanmohammadi, S. and Pakseresht, A., 2021. A novel multi-generation energy system based on geothermal energy source: Thermo-economic evaluation and optimization, *Energy Conversion and Management,* 230, pp. 113829. Doi:10.1016/j.enconman.2021.113829
23. Loni, R. a., Asli-Ardeh, E. A., Ghobadian, B., Kasaeian, A. and Gorjian, S., 2017. Thermodynamic analysis of a solar dish receiver using different nanofluids, *Energy,* 133, pp. 749-760. Doi:10.1016/j.energy.2017.05.016
24. Khan, M. S., Abid, M., Ali, H. M., Amber, K. P., Bashir, M. A. and Javed, S., 2019. Comparative performance assessment of solar dish assisted s-CO2 Brayton cycle using nanofluids, *Applied Thermal Engineering,* 148, pp. 295-306. Doi:10.1016/j.applthermaleng.2018.11.021
25. Al-Hamed, K. and Dincer, I., 2019. Investigation of a concentrated solar-geothermal integrated system with a combined ejector-absorption refrigeration cycle for a small community,

International Journal of Refrigeration, 106, pp. 407-426. Doi:10.1016/j.ijrefrig.2019.06.026

26. Alirahmi, S. M., Rostami, M. and Farajollahi, A. H., 2020. Multi-criteria design optimization and thermodynamic analysis of a novel multi-generation energy system for hydrogen, cooling, heating, power, and freshwater, *International Journal of Hydrogen Energy*, 45(30), pp. 15047-15062. Doi:10.1016/j.ijhydene.2020.03.235
27. Al-Sulaiman, F. A., 2014. Exergy analysis of parabolic trough solar collectors integrated with combined steam and organic Rankine cycles, *Energy Conversion and Management*, 77, pp. 441-449. Doi:10.1016/j.enconman.2013.10.013
28. Alirahmi, S. M., Dabbagh, S. R., Ahmadi, P. and Wongwises, S., 2020. Multi-objective design optimization of a multi-generation energy system based on geothermal and solar energy, *Energy Conversion and Management*, 205, pp. 112426. Doi:10.1016/j.enconman.2019.112426
29. Yüksel, Y. E., 2018. Thermodynamic assessment of modified Organic Rankine Cycle integrated with parabolic trough collector for hydrogen production, *International Journal of Hydrogen Energy*, 43(11), pp. 5832-5841. Doi:10.1016/j.ijhydene.2017.09.164
30. Sarabchi, N., Mahmoudi, S. S., Yari, M. and Farzi, A., 2019. Exergoeconomic analysis and optimization of a novel hybrid cogeneration system: High-temperature proton exchange membrane fuel cell/Kalina cycle, driven by solar energy, *Energy Conversion and Management*, 190, pp. 14-33. Doi:10.1016/j.enconman.2019.03.037
31. Nafey, A. and Sharaf, M., 2010. Combined solar organic Rankine cycle with reverse osmosis desalination process: Energy, exergy, and cost evaluations, *Renewable Energy*, 35(11), pp. 2571-2580. Doi:10.1016/j.renene.2010.03.034
32. Nemati, A., Sadeghi, M. and Yari, M., 2017. Exergoeconomic analysis and multi-objective optimization of a marine engine waste heat driven RO desalination system integrated with an organic Rankine cycle using zeotropic working fluid, *Desalination*, 422, pp. 113-123. Doi:10.1016/j.desal.2017.08.012
33. Aliahmadi, M., Moosavi, A. and Sadrhosseini, H., 2021. Multi-objective optimization of regenerative ORC system integrated with thermoelectric generators for low-temperature waste heat recovery, *Energy Reports*, 7, pp. 300-313. Doi:10.1016/j.egyr.2020.12.035
34. Habibzadeh, A., Rashidi, M. and Galanis, N., 2013. Analysis of a combined power and ejector-refrigeration cycle using low temperature heat, *Energy Conversion and Management*, 65, pp. 381-391. Doi:10.1016/j.enconman.2012.08.020
35. Rostamnejad Takleh, H. and Zare, V., 2021. Proposal and thermoeconomic evaluation with reliability considerations of geothermal driven trigeneration systems with independent operations for summer and winter, *International Journal of Refrigeration*, 127, pp. 34-46. Doi:10.1016/j.ijrefrig.2020.12.033
36. Kalogirou, S. A., 2013. Solar energy engineering: processes and systems. Academic press. 0123972566:0123972566.
37. Abdolalipouradl, M., Khalilarya, S. and Jafarmadar, S., 2019. Energy and exergy analysis of a new power, heating, oxygen and hydrogen cogeneration cycle based on the sabalan geothermal wells, *International Journal of Engineering, Transactions C: Aspects*, 32(3), pp. 445-450. Doi:10.5829/ije.2019.32.03c.13
38. Xi, Z., Eshaghi, S. and Sardari, F., 2021. Energy, exergy, and exergoeconomic analysis of a polygeneration system driven by solar energy with a thermal energy storage tank for power, heating, and freshwater production, *Journal of Energy Storage*, 36, pp. 102429. Doi:10.1016/j.est.2021.102429
39. Szargut, J., 2005. Exergy method: technical and ecological applications. WIT Press. ISBN: 1853127531.
40. Assareh, E., Alirahmi, S. M. and Ahmadi, P., 2021. A Sustainable model for the integration of solar and geothermal energy boosted with thermoelectric generators (TEGs) for electricity, cooling and desalination purpose, *Geothermics*, 92, pp. 102042. Doi:10.1016/j.geothermics.2021.102042
41. Akrami, E., Chitsaz, A., Nami, H. and Mahmoudi, S., 2017. Energetic and exergoeconomic assessment of a multi-generation energy system based on indirect use of geothermal energy, *Energy*, 124, pp. 625-639. Doi:10.1016/j.energy.2017.02.006
42. Ahmadi, P., Dincer, I. and Rosen, M. A., 2014. Multi-objective optimization of a novel solar-based multigeneration energy system, *Solar Energy*, 108, pp. 576-591. Doi:10.1016/j.solener.2014.07.022
43. Yu, Z., Su, R. and Feng, C., 2020. Thermodynamic analysis and multi-objective optimization of a novel power generation system driven by geothermal energy, *Energy*, 199, pp. 117381. Doi:10.1016/j.energy.2020.117381

Persian Abstract

چکیده

در این مطالعه، منابع انرژی تجدیدپذیر شامل یک کلکتور سهموی خورشیدی با دمای بالا و آب زمین گرمایی با یک چرخه کالینای اصلاح شده، یک چرخه ترکیبیORC-ERC، یک الکترولایز، یک واحد نمک‌زدایی RO و یک آبگرمکن خانگی ترکیب شده‌اند مورد بررسی قرار گرفته‌اند. نانوذرات SiO_2 و TiO_2 حل شده در Therminol VP1 به عنوان سیال کاری کلکتور خورشیدی استفاده شده است. تجزیه و تحلیل مقایسه‌ای سیال عامل‌های معرفی شده از نقطه نظر انرژی، اگزرژی و همچنین تحلیل هزینه برای ارزیابی کارآیی آنها انجام می‌گردد. مقدار تابش خورشیدی، دمای محیط و دمای ورودی کلکتور پارامترهایی بودند که برای بررسی اثرات آنها بر بازده انرژی و اگزرژی، دمای خروجی کلکتور خورشیدی، نرخ تولید هیدروژن و نرخ تولید آب شیرین مورد بررسی قرار گرفتند. بالاترین دمای تولید شده خروجی کلکتور خورشیدی ۶۹۳/۸ کلوین با استفاده از نانوسیال Therminol VP1/SiO_2 به دست آمد. حداکثر بازده انرژی و اگزرژی سیستم پیشنهادی به ترتیب ۳۶/۶۹ درصد و ۱۷/۷۶ درصد بود. علاوه بر این، مشخص شد که با افزایش دمای ورودی کلکتور خورشیدی، نرخ تولید هیدروژن کاهش می‌یابد، در حالی که نرخ تولید آب افزایش خواهدیافت.